ELSEVIER

Agricultural and Forest Meteorology 93 (1999) 259–282

AGRICULTURAL AND FOREST METEOROLOGY

Wind and remnant tree sway in forest cutblocks. III. a windflow model to diagnose spatial variation

John D. Wilson*, Thomas K. Flesch

Department of Earth and Atmospheric Sciences, University of Alberta, Edmonton, Alberta, Canada T6G 2E3

Received 18 March 1998; accepted 15 September 1998

Abstract

Root-mean-square tree sway angle (σ_θ) can be related to the r.m.s. value ($\sigma_{u|u|}$) of the wind 'force' $u|u|$, specified nearby. Therefore the spatial pattern of wind statistics over the landscape, if known, arguably maps the relative risk of windthrow – suggesting a wind model can provide the basis to interpret spatial patterns of windthrow, and guide strategies with respect to that concern. To test this idea, we adopt a simple flow model able to describe both the mean wind (U) and kinetic energy of the turbulence (k), viz. Reynolds' equations closed using eddy-viscosity $K \propto \lambda k^{1/2}$, where λ is the turbulence lengthscale. We first compare this model with others' measurements of wind near forest edges, then simulate our own observations, which spanned arrays of cutblocks and intervening forest blocks in the Boreal forest (periodic spacing $1.7h$ or $6.1h$, where h is mean tree height). We show that the model predicts well the spatial variation of the mean windspeed and turbulent kinetic energy, these being the wind statistics having greatest impact upon tree sway. Model-implied spatial patterns of r.m.s. wind force ($\sigma_{u|u|}$) agree closely with those observed, and in conjunction with a tree-motion model, imply tree sway (σ_θ).

Keywords: Forest wind model; (wind in) forest clearings; Windbreaks; Tree sway

1. Introduction

Management trials in the boreal mixedwood forest of northern Canada are evaluating felling practises that, at the time of aspen harvest, preserve the spruce understory ('released spruce') for later cutting. It is considered necessary to leave uncut or partially-cut forest strips to shelter the selectively-cut zones, because the previously-sheltered remnant spruce are very vulnerable to windthrow. An overall description of this long-term, practically-oriented project, which is being carried out near Manning (Alberta) by Forestry Canada and partners, is given by Navratil et al. (1994). The work we report here (and in companion papers, Flesch and Wilson, 1999a, b) was initiated in the hope of interpreting the observed *spatial variation* of tree windthrow across such arrays of cutblocks, so as to permit generalisation. It involves our own measurements of turbulence and tree sway in two cutblocks, each the leeward member of a periodic series; an analysis of the response of instrumented trees to the wind forcing; and, in this paper, an attempt to establish a framework for generalisation of our findings by numerically modelling the winds.

The link between tree sway statistics and wind statistics is discussed at length by Flesch and Wilson

*Corresponding author. Tel.: +1-403-492-3265; fax: +1-403-492-2030

0168-1923/99/$ – see front matter
PII: S0168-1923(98)00121-X

(1999b). Briefly, we treated the tree as a rigid rod, free to swing about a ground-level pivot in response to the wind force, but under the moderation of an angular spring and damper. We derived a transfer function relating the short-term power spectrum S_θ of tree angular displacement (θ) to the concurrent power spectrum $S_{u|u|}$ of the wind force $u|u|$, where u is the instantaneous alongwind velocity component, measured nearby. By 'short-term' statistics, we mean statistical properties (standard deviations of tree sway angle σ_θ and of wind force $\sigma_{u|u|}$, variance spectra S_θ, $S_{u|u|}$, etc.) defined by a sample taken over about 15 to 60 min., such intervals being sufficiently short that 'external' or large-scale conditions are roughly constant, but sufficiently long that many 'cycles' of the rapid turbulent variations are captured. Thus the 'view' of our windthrow analysis consists of (say) 30 min. snapshots, from which a longer-term view may be constructed by integration; and the fluctuating (turbulent) variables, e.g. the alongwind velocity u, are decomposed

$$u(x,y,z,t) = U(x,y,z) + u'(x,y,z,t) \qquad (1)$$

into sums of the average (in this case, the mean alongwind velocity U, a function of position only) and the instantaneous deviation (or fluctuation, here u') from it. This terminology (upper-case for mean values; prime for fluctuation from average) will apply throughout our paper.

Returning to our tree sway model, the wind-force spectrum $S_{u|u|}$ was observed not *at* the 'subject' remnant tree, but merely, at the same *alongwind* location relative to the upwind edge of the cutblock, and at a convenient, arbitrary height (9 m). We found that *normalized* wind force spectra $S_{u|u|}/\sigma^2_{u|u|}$ were similar at all points across the cutblocks (i.e. practically invariant), so that the sway (σ_θ) of a tree, no matter where located, could be definitively related to $\sigma^2_{u|u|}$ at that point. But in turn, the force-variance $\sigma^2_{u|u|}$ can be determined from the lowest order statistics of the wind

$$\sigma^2_{u|u|} \approx \sigma^2_{uu} \equiv \sigma^4_u \left(\mathrm{Kt}_u - 1 + 4\left(\frac{U}{\sigma_u}\right)^2 + 4\left(\frac{U}{\sigma_u}\right)\mathrm{Sk}_u \right) \qquad (2)$$

where the right-hand equality is exact. Within our framework then, the wind statistics governing root-mean-square (r.m.s.) tree sway are: mean U, variance σ^2_u, skewness Sk_u, and kurtosis Kt_u. A sensitivity analysis (see Appendix A) indicates that under conditions typical of the flow in our Manning cutblocks ($\mathrm{Sk}_u \approx 1$, $\mathrm{Kt}_u \approx 4$), spatial modulation of the wind-force variance (and thus of σ^2_θ) is controlled, in order of importance, by spatial variation in the velocity variance σ^2_u (one component of the turbulent kinetic energy[1]), and in the mean velocity U. Thus for the remainder of this paper, our focus is on modelling the spatial variation, around and about forest edges, of these principal wind and turbulence statistics, U and k. As regards the connexion of our method to the practical issue of tree windthrow, by hypothesizing that the *spatial pattern* of wind statistics implies the corresponding *spatial pattern* of windthrow, we obviously are assuming that the key factor in the cross-landscape *variation* of treefall susceptibility is the wind forcing, rather than any systematic variation in soil conditions, rooting depth, tree health, etc. It is also implicit that we presume *extreme* tree displacements (or wind forces) scale with the standard deviation σ_θ (or with $\sigma_{u|u|}$).

Having motivated our focus on mean wind (U) and turbulence (k) in forest clearings, we now review previous efforts to model forest edge flows; describe a numerical windflow model, developed by Wilson et al. (1998) specifically for the description of disturbed canopy winds; compare simulations using that model against others' observations of forest-edge flows; and finally simulate the spatial pattern of the wind and turbulence in our cutblocks at Manning for comparison with our observations.

2. Windflow across forest boundaries, and models thereof

We have elsewhere (Flesch and Wilson, 1999a) discussed the experiments to date on forest edge flows, in comparison with our own. Here we consider only the issue of whether or not one might expect to see universal patterns across such experiments.

[1] Turbulent kinetic energy (TKE, k) is defined as $k = \frac{1}{2}(\sigma^2_u + \sigma^2_v + \sigma^2_w)$. The flow model we shall describe does not partition k into its components, so we have assumed that *equilibrium* partitioning prevails everywhere throughout disturbed flows: i.e. that everywhere $\sigma^2_u = \alpha_u k$, where α_u is a constant, given in Appendix C.

Shinn (1971) analysed his own and others' experiments on forest edge flow. His observations of wind in *uniform* canopies are also important: he showed that due to the Coriolis force there occurs a large swing (about 80°) in mean wind direction between tree-top level and the base of the canopy (see Appendix B for a discussion), and for this reason we anticipate that the Coriolis force ought to be included in any complete analysis or model of forest edge flow.

Shinn demonstrated that mean windspeed profiles in the forest entry region from a number of field experiments on forest-wall flow formed a fairly consistent pattern, a pattern which, not withstanding the above caution with respect to Coriolis effects, resembled the corresponding pattern from a wind tunnel experiment: at low levels a jet penetrates the canopy, decaying by about $x/h = 10$. Shinn normalised the observations using lengthscale h and velocity scale $U_0(h)$, the windspeed at canopy height some distance upwind from the forest wall. Differences not erased by the normalisation are of course expected, for in general, even in neutrally-stratified flow at a forest edge having along-edge (y) symmetry, one expects on the basis of dimensional analysis a similarity relationship at least as complex as

$$\frac{U}{U_{\mathrm{ref}}} = F\left(\frac{x}{h}, \frac{z}{h}, \frac{\delta}{h}, \frac{z_{\mathrm{oc}}}{h}, c_{\mathrm{d}}ah, \frac{f}{c_{\mathrm{d}}aU_{\mathrm{ref}}}\right) \qquad (3)$$

where F is an unknown function of its bracketed (and dimensionless) arguments; U_{ref} is the normalising velocity scale; δ is boundary layer depth; z_{oc} is the effective surface roughness length in the clearing; $c_{\mathrm{d}}ah$ is a bulk (constant) drag coefficient characterising the forest block(s), $a = a(x, z)$ being the forest drag area density, (m^{-1}); and f is the Coriolis parameter. In general, atmospheric stratification and the *vertical distributions* of drag coefficient and foliage area density probably play a role, implying we could add, as further dimensionless arguments of the unknown function F, the factors h/L_{MO} (where L_{MO} is the Monin–Obukhov length), $c_{\mathrm{d}}(z/h)$, and $ah(z/h)$. And because the drag coefficient may be Reynolds-number dependent, we might also add a Reynolds number $U_{\mathrm{ref}}h/\nu$, ν being the kinematic viscosity of the air. Our point here is that by no means ought one to *expect* there exists a universal pattern (of the normalised flow variables) across differing forest edge flows.

2.1. Background on numerical simulation of turbulent flows

Simulations of disturbed micrometeorological flows are most often based on numerical integration of the Reynolds equations, which are obtained by averaging the Navier–Stokes equations so as to obtain governing equations for the flow *statistics* (see Hinze, 1975 or almost any text on turbulence or micrometeorology). If the flow has (statistical) symmetry along one spatial axis (say, y-axis), the Reynolds equation expressing conservation of mean alongwind (x-axis) momentum can be written as

$$\frac{\partial}{\partial x}(U^2 + \sigma_u^2) + \frac{\partial}{\partial z}(UW + \tau) = -\frac{1}{\rho}\frac{\partial P}{\partial x} + \Phi_u \qquad (4)$$

where U and W are the mean alongwind and vertical (z-axis) velocities; P is the mean pressure; ρ is the mean air density; Φ_u represents the Coriolis force and drag of vegetation on the flow; and $\tau = \langle u'w' \rangle$ is the statistical covariance between u-fluctuations and w-fluctuations, which in physical terms is the turbulent shearing stress, known as the Reynolds stress. We need not elaborate on Eq. (4) at this point (it reappears later in approximate form as Eq. (7)), except to mention that whereas this is an equation 'for' the *mean* x-wise momentum, i.e. for velocity U, its derivation has introduced spatial derivatives of higher (and unknown) statistics of the velocity field, namely of the variance σ_u^2 and of the covariance $\tau = \langle u'w' \rangle$. These 'stress-gradients,' physically, are *forces*, 'felt by' the mean flow: and in particular the term $\partial\tau/\partial z$ in Eq. (4) is crucial in most turbulent flows. In order to progress, one has necessarily to introduce a hypothesis with respect to the Reynolds stresses (a 'closure hypothesis'). The oldest and simplest such hypothesis is the eddy-viscosity closure, often called 'K-theory,' or 'first-order closure',

$$\tau = -K\left(\frac{\partial U}{\partial x} + \frac{\partial W}{\partial z}\right) \qquad (5)$$

Here the shear stress is assumed to be determined by the mean strain, in analogy with Newton's law for the *viscous* shear stresses. K is the 'eddy viscosity,' and may always be regarded as the product ($K = \lambda\Gamma$) of a turbulence lengthscale (λ) and velocity scale (Γ). Its specification, auspicious or otherwise, is often the key to success of a flow simulation. In the simplest flows, it

can be prescribed algebraically. For example in the neutrally-stratified and undisturbed atmospheric surface layer (NSL), at heights $z \gg z_0$, z_0 being the roughness length, it is well established that $K = k_v u_* z$, where $k_v \approx 0.4$ is von Karman's constant, and u_* is the friction velocity; i.e. in the ideal NSL, $\lambda = k_v z$ and $\Gamma = u_*$. In more complex flows, one might obtain the velocity scale Γ from the mean velocity shear ($\Gamma = \lambda \partial U/\partial z$; Prandtl's closure); or, one might assume Γ to be proportional to $k^{1/2}$, and so obtain it by including (as one of the equations integrated) the transport equation for k (Prandtl–Kolmogorov closure). One step higher in closure-complexity, falls the popular 'k–ε' model, wherein the lengthscale λ too is *calculated*, as $\lambda \propto k^{3/2}/\varepsilon$, by also including a transport equation for the rate (ε) of dissipation (by viscous forces) of TKE to heat. Or, one may abandon K-theory altogether, and include a simplified budget equation for τ, which can be derived from the Navier–Stokes equations ('higher-order closure'). For reasons discussed by Wilson et al. (1998), our preference in treating disturbed canopy flows is to use their variant of the K-closure, arguably the simplest applicable.

2.2. Simulations of forest edge flow

Apparently the earliest numerical simulations of windflow through a forest edge were by Li et al. (1990) (hereafter LLM), and by Svensson and Haggkvist (1990). In both cases K-theory was used to relate the shear stress τ to the mean velocity gradients. However to introduce the possibility of counter-gradient turbulent momentum transport (i.e. to allow that τ may transport mean momentum from regions of *low* mean speed to regions of *high* mean speed, which can happen in a flow of this type and is disallowed by K-theory), LLM used a heuristic modification of Eq. (5), first given by Li et al. (1985). The shear stress gradient in Eq. (4) was parametrized as

$$\frac{\partial \tau}{\partial z} = -\frac{\partial}{\partial z}\left(K\left(\frac{\partial U}{\partial z} + \frac{\partial W}{\partial x}\right)\right) - c(U(h) - U(z)) \tag{6}$$

where c is an empirical coefficient (presumably this additional term was included only within the canopy). The eddy viscosity was calculated using Prandtl's mixing-length formulation.

LLM simulated the field experiments of Raynor (1971), who reported cup windspeeds measured near the edge ($x = 0$) of a pine forest of height $h = 10.5$ m. For flow *into* the forest, the model replicated generally to within a few percent the observed windspeeds, which showed an abrupt but regular transition from the open-field profile-form ($U \propto \ln_e z$), to a canopy-type (inflexion-point) wind profile. The model reproduced an observed jet of high windspeeds penetrating into the canopy at low level (where the leaf area density was small) and visible as a secondary maximum in windspeed even at a distance $10h$ into the forest from the edge, but the authors did not state whether this feature depended on their having included the extra source in the U-momentum equation. In the case of flow *from* the forest, again model performance was excellent, reproducing the canopy wind profiles upstream from the edge, which though self-similar in form showed slight acceleration as the edge was approached. For both directions of flow, the authors emphasized the sizeable pressure gradients affecting the flow near the forest edge (such pressure gradients apparently exert a large influence on the flow in our periodic cutblocks). The LLM model was later applied by Miller et al. (1991) to simulate forest clearings.

In a study concerned with efficient parametrization of forest effects in mesoscale models, Schilling (1991) reported the results of a low-resolution ($\Delta x = 500$ m) simulation of flow through a wide clearing (width $X_C = 8$ km). Schilling adopted the Prandtl–Kolmogorov form of K-theory, i.e. $K \propto \lambda k^{1/2}$ (velocity scale from TKE budget; imposed lengthscale λ), but without adaptation of the lengthscale to account for the presence of the canopy. As our instrumented clearings are typified by $X_C/h = 2$–6, whereas Schilling's clearing is of entirely different aspect ratio $X_C/h = 400$, our simulations are completely different in scale.

Green et al. (1994) studied the flow through a stand of forest whose crosswind extent was $10h$. They reported qualitative agreement between the mean velocity and the TKE as observed in a wind tunnel simulation, and as according to a numerical model based on a modified k–ε closure. Owing to the drag of vegetation, application of the k–ε model in presence of a canopy requires specification of the scale-range covered by TKE, and entails heuristic modifications of the k- and ε-equations. Such adjustments are arbi-

trary and ambiguous, and can have a large (100% or more) impact on numerical results, particularly for TKE (see Green et al., 1994 and Liu et al., 1996 for forest edge flow; and Wang and Takle, 1996 for windbreak flow).

Liu et al. (1996) (hereafter LCBN) used the k–ε model to simulate the flow from a uniformly forested region into a clearing, comparing their model with wind-tunnel observations of Chen et al. (1995). Like Green et al. (1994), but slightly differently, they modified the TKE and dissipation equations of the standard k–ε model, in order to account for the influence of vegetation. Viewed on the large scale (5×35 h; their Figs. 2 and 3), the modelled mean velocity field (U) appears to be in excellent agreement with the observations, though it is the nature of side-by-side vector plots and contour plots to emphasize similarity rather than difference. Their Fig. 4 compares modelled and measured vertical U-profiles, showing excellent quantitative conformity of model and data, except for sizeable discrepancies (order 100%) within about $3h$ from the forest edge. In that region the numerical model produced mean flow reversal near ground, while flutter-flags in the wind tunnel indicated intermittently reverse flow. The hot-film anemometers rectify reverse-velocities, so were in error in this region. Turbulent kinetic energy was also simulated well, but only provided that sources in the k- and ε-equations were adjusted. Without that step errors in k of order 100% occurred (their Fig. 9). LCBN concluded their model was ''less satisfactory in describing turbulent airflow over short distances downwind of forest edges''.

Relative to the work described above, our present examination of flow in discontinuous forests has a more specific end in view: can we model the spatial variation of the lower order wind statistics sufficiently well that the implied spatial patterns in the r.m.s. wind force $\sigma_{u|u|}$ and (by virtue of our tree-sway model) tree sway σ_θ are realistic? While to all appearances the LCBN model may be quite capable of answering the question, we chose to investigate the matter using a model based on the simplest workable turbulence closure for disturbed canopy flows (Wilson et al., 1998; hereafter WFR), which through direct algebraic specification of the lengthscale, sidesteps the ambiguities of sources in the k- and ε-equations. The WFR model has already been tested, for both uniform and disturbed canopy flows, more exhaustively than modified k–ε type models. In Section 3 we shall briefly describe the WFR model. In Sections 4 and 5 we show that without alteration, other than to parametrize the lengthscale adjustment within clearings, the WFR model provides good simulations of others' experiments on clearing flows. In Section 6 we compare the WFR model against our measurements in the Manning cutblocks.

3. Windflow model

We consider only flows whose mean properties are constant along an axis (y) oriented parallel to forest edges, and assume the mean wind is oriented approximately perpendicularly across the edges, i.e. along the x-axis. When we apply our model to simulate our cutblock flows at Manning, that symmetry assumption is not exactly valid, for if X_C, Y_C denote the along-wind- and crosswind-widths of the cutblocks, then the aspect ratio Y_C/X_C was not very large (3, 15 for the wide and narrow cutblocks, respectively). However exploratory simulations with a 3-dimensional generalisation of our model (A. Tuzet, pers. comm.), permitting to account for finite aspect ratio of the clearing and/or for winds at oblique incidence, suggest our present neglect of y-dependence is not very consequential.

The windflow model is a straightforward adaptation of that applied by Wilson et al. (1998) to calculate variation of the wind and turbulence in a model plant canopy on a wind-tunnel ridge. Finding it the simplest adequate treatment of disturbed canopy flow, WFR chose a first-order turbulence closure which has seen use in just about every type of micrometeorological flow (e.g. the nocturnal boundary layer; Delage, 1974); the eddy viscosity is written $K \propto k^{1/2}\lambda$, where the turbulent kinetic energy (k) is obtained from a simplified transport equation, and the turbulence lengthscale λ is specified algebraically. Changes to the WFR model necessary for our present purposes are two-fold in origin. Firstly, we require a flow domain extending several kilometers alongwind over the periodic cutblocks, and so must simulate a deep layer of the Planetary Boundary Layer (PBL): thus Coriolis effects couple the mean alongwind velocity component (U) to the crosswind velocity (V). Secondly,

variation of the lengthscale across the cutblock-forest block boundaries must be parameterised. In addition to these changes, because the skewness of windspeed influences tree motion, we added an approximate transport equation for the third moment of the velocity fluctuation (Appendix C).

Detailed explanation of the model equations and numerical procedure is given by WFR, and so we shall give only a brief description here. As our ultimate objective is the understanding or interpretation of patterns of tree windthrow, and (our own) observations are from periods of strong winds, we need not be concerned with temperature-stratification. We solved simplified U, V, W-momentum equations, that represent only what are (according to experience) the dominant terms (advection by the mean flow; pressure gradient; drag on trees; and divergence of the vertical turbulent momentum flux). These equations, cast in dimensionless form (using lengthscale h, and a velocity scale U_G defined below) are

$$\frac{\partial}{\partial x}\left(U^2 - K_a\frac{\partial U}{\partial x}\right) + \frac{\partial}{\partial z}\left(UW - K\frac{\partial U}{\partial z}\right) = f(V - V_G) - \frac{\partial P}{\partial x} - c_d a^* U\sqrt{U^2+V^2} \quad (7)$$

$$\frac{\partial}{\partial x}\left(UV - K_a\frac{\partial V}{\partial x}\right) + \frac{\partial}{\partial z}\left(VW - K\frac{\partial V}{\partial z}\right) = f(U_G - U) - \frac{\partial P}{\partial y} - c_d a^* V\sqrt{U^2+V^2} \quad (8)$$

$$\frac{\partial}{\partial x}\left(UW - K_a\frac{\partial W}{\partial x}\right) + \frac{\partial}{\partial z}\left(W^2 - K_a\frac{\partial W}{\partial z}\right) = -\frac{\partial P}{\partial z} \quad (9)$$

The incompressible continuity equation

$$\frac{\partial U}{\partial x} + \frac{\partial W}{\partial z} = 0 \quad (10)$$

also applies ($\partial_y V = 0$ by assumption). In the momentum equations P is the local mean pressure perturbation (normalised on ρU_G^2); $f^* = fh/U_G$, where f is the Coriolis parameter; fU_G, fV_G are the components of the large-scale background pressure gradient, where (U_G, V_G) are the components of a nominal 'Geostrophic' wind aloft; c_d is the bulk drag coefficient of trees; and $a^* = ah$, where a is the area density ($m^2\,m^{-3}$) of tree parts (variable through cutblocks and forest blocks). K_a is a small artificial viscosity/diffusivity, included to ensure numerical stability, while K is the 'true' eddy viscosity, estimated as

$$K = \lambda(x,z)\sqrt{c_e k(x,z)} \quad (11)$$

In Eq. (11) the constant $c_e = u_{*0}^2/k_0(h)$, where $-u_{*0}^2, k_0(h)$ are the shear stress and the TKE at height $z = h$ under the reference condition of a uniform forest canopy; $\lambda(x,z)$ is a turbulence lengthscale; and $k(x,z)$ is the TKE determined from the approximate TKE budget

$$\frac{\partial}{\partial x}\left(Uk - K_a\frac{\partial k}{\partial x}\right) + \frac{\partial}{\partial z}\left(Wk - \mu K\frac{\partial k}{\partial z}\right) = K\left(\left(\frac{\partial U}{\partial z}\right)^2 + \left(\frac{\partial V}{\partial z}\right)^2\right) - \varepsilon \quad (12)$$

The constant μ represents the ratio of the effective eddy diffusivity for TKE to the eddy viscosity. The TKE dissipation rate (ε) was specified as

$$\varepsilon = \max\left[\frac{(c_e k)^{3/2}}{\lambda}, \alpha c_d a^*\sqrt{U^2+V^2}\,k\right] \quad (13)$$

where within the canopy the wake conversion term dominates. The rationale for this closure is given by WFR.

3.1. Specification of the lengthscale

Like Li et al. (1990), we anticipated it would be necessary for forest-edge flows to interpolate for the lengthscale between two limiting cases: the infinite open plain lengthscale λ_P, and the infinite-forest lengthscale λ_F. However our specification of λ_F differs from theirs, and we interpolated differently. Over flat, open ground during neutral stratification, the lengthscale may be parametrized as

$$\frac{1}{\lambda_P} = \frac{1}{k_v z} + \frac{1}{L_\infty} \quad (14)$$

where L_∞ is Blakadar's (1962) lengthscale, limiting growth of the lengthscale in the PBL. In dimensional terms, L_∞ is often estimated (e.g. Delage, 1974) as approximately

$$L_\infty = 0.0004\frac{U_G}{f} \quad (15)$$

Rather than use (as did Li et al.) an in-forest lengthscale (λ_F) based on an equilibrium parametrization tuned to canopy area density, we followed WFR

and wrote $\lambda = \max(\lambda_i, \lambda_o)$, where

$$\frac{1}{\lambda_i} = \frac{1}{k_v z} + \frac{1}{\lambda_c}, \frac{1}{\lambda_o} = \frac{1}{k_v(z-d)} + \frac{1}{L_\infty} \qquad (16)$$

λ_c is a canopy 'shear length scale',

$$\lambda_c = c\sqrt{k(h)}\left(\frac{\partial S}{\partial z}\right)_h^{-1} \qquad (17)$$

where $S = (U^2 + V^2)^{1/2}$ is the 'cup' windspeed; this parametrization links the lengthscale in and near the canopy to the wind shear at canopy top, which may vary substantially across forest blocks.

These two limiting expressions for the lengthscale (infinite clearing, infinite forest) may be conveniently blended into a universal expression valid at all locations, simply by replacing the displacement length d in Eq. (16) with an effective displacement length d_e,

$$d_e = \frac{d}{1 + \gamma(x - x_0)} \qquad (18)$$

where $d(\approx \frac{2}{3}h)$ is the equilibrium displacement length, $x_0(\leq x)$ denotes the leeward edge of the forest block lying immediately upwind of the clearing in question, and γ is an empirical constant. Upon passage from clearing back into forest, we immediately restored the equilibrium displacement length, $d_e = d$. In general, our simulations were rather insensitive to our treatment of the lengthscale transition, although the calculated pattern of TKE for the Manning cutblock flow showed some reaction to the choices made.

3.2. Specifying adjustable constants

The artificial diffusivity was set at $K_a = 0.001hU_G$, and had insignificant effect on the simulations other than to ensure numerical stability.

The WFR closure involves three closure constants. These were optimised by WFR ($c = \alpha = 1$, $\mu = 0.2$) by matching equilibrium solutions of the equations to wind tunnel observations in and above a uniform model canopy, and were not changed in the present work. Well above the canopy it would be more consistent with others' shear layer simulations to set the ratio (μ) of the diffusivity for TKE to the eddy viscosity as $\mu = 1$; but our simulations are focused on flow changes very near ground, and we incorporated the outer boundary-layer simply as an appropriate domain within which those changes occurred, not as an end in itself.

Other rather familiar parameters have appeared in our model equations, as constants which we want to clearly distinguish from the closure parameters – to emphasize that the success of our simulations does not depend on any flexibility in their specification: they are c_e, and the Coriolis parameter, f. Typically in flow above a uniform canopy, $\sigma_{u,v,w}/u_{*0} \approx 2{,}2{,}1.3$, implying $c_e \approx 0.2$: we used $c_e = 0.18$. And we set $f^* = (hf/U_G) = 1.5 \times 10^{-4}$, which represents moderately windy conditions at middle latitudes over a tall forest.

It only remained in our present applications of the windflow model to specify the lengthscale adjustment parameter (γ); and the forest-specific canopy area density $a(z)$, and drag coefficient $c_d(z)$. These choices will be given for each case study.

3.3. Numerical details and boundary conditions

Numerical details specific to each case-study will be given in following sections, but we shall here cover the general scheme we employed in integrating the governing equations.

We used Patankar's (1980) well-documented Semi-Implicit Method for Pressure-Linked Equations (SIMPLE) to solve the equations. Inflow profiles of U, V, k were obtained as equilibrium ($\partial/\partial x = 0$) solutions of the equations (with or without a forest, as appropriate), and imposed far upwind from the region of interest. Far downwind, at the outflow boundary, we set $\partial U/\partial x = \partial V/\partial x = \partial k/\partial x = W = 0$.

3.3.1. Upper boundary conditions

For the Manning simulations, we set $U = U_G = 1$, $V = V_G$, $W = k = 0$. All velocities were scaled on U_G, thus the specification $U_G = 1$; V_G was adjusted so that near the top of the canopy, $V \approx 0$.

For simulation of the wind-tunnel flow, we placed the uppermost W gridpoint at the top of the domain, so that the shear stress along that boundary is the required condition on the U-momentum balance. Either we specified that shear stress aloft as undisturbed (u_{*0}^2) and constituting the velocity scale for the simulation; or, if we wished to properly account for stress and TKE gradients at $z > h$ in the incident flow, we incorporated an effective background pressure gradient, and specified the stress aloft as vanishing; i.e. if

the measured stress gradient above the canopy was $(\partial\tau/\partial z)_0$ then we applied a background pressure gradient $(1/\rho)(\partial P/\partial x)_0 = (\partial\tau/\partial z)_0$ throughout the layer $z \leq z_{mx} = h + \tau(h)/(\partial\tau/\partial z)_0$ so as to give rise to a linear variation of shear stress from 0 at $z = z_{mx}$ to $\tau(h)$ at $z = h$.

3.3.2. Lower boundary conditions

Two choices were explored for the lower boundary conditions. Initially, we set the lowest U,V gridpoints on ground, where $U = V = 0$. Then the lowest vertical velocity and TKE gridpoints lie above ground, within normal control volumes, for which the required boundary condition is a specification of the *flux* to ground. We set those fluxes to zero. This direct imposition of the no-slip condition obviates necessity to assume a 'wall function' relationship between surface shear-stress and near-wall windspeed, and seems the better choice within a fully forested domain.

However far downwind in sufficiently wide clearings, naturally one expects any reasonable model to develop the usual semi-logarithmic equilibrium wind profile; and if one did not *impose* a roughness length in the clearings, then a value implicit to the model itself, but which is unknown a priori, must eventuate. To circumvent that curious ambiguity, in all reported simulations we have set the lowest vertical velocity and TKE gridpoints on ground. Consequently the lowest U,V gridpoints lay above ground, at $z = z_P$, and a condition on the corresponding vertical momentum fluxes to ground was required. We specified $\langle u'w' \rangle = -u_{*u}^2$, $\langle v'w' \rangle = -u_{*v}^2$, where

$$u_{*u} = k_v U_P / \ln\left(\frac{z_P}{z_0}\right), \quad u_{*v} = k_v V_P / \ln\left(\frac{z_P}{z_0}\right),$$
$$u_*^2 = u_{*u}^2 + u_{*v}^2 \tag{19}$$

Of course, these wall relationships are not valid within the canopy (nor for that matter in regions of highly-disturbed flow), but as the shear stress on ground beneath a dense canopy is very small, its miscalculation (by the above relationships) is expected to carry negligible penalty. It is interesting to note that simulations under the two alternatives, i.e. explicit imposition (or otherwise) of the clearing roughness length, did not differ sufficiently to warrant giving the matter further attention.

As the lower boundary condition on TKE in conjunction with Eq. (19), we adopted the equilibrium relationship $k_{gnd} = u_*^2/c_e$. The alternative prescription $(\partial k/\partial z)_0 = 0$ performed neither better nor worse.

3.3.3. Convergence criterion

SIMPLE ensures that the governing equations, in their integral forms which express the balance of sources within each control volume against the net flux across the control-volume surface, are satisfied to within machine precision (in each such volume). Iterative refinement of all fields was continued until the integral form of the U-momentum Eq. (7), covering the entire flow domain, was satisfied to within 1% of the total forest drag.

3.4. Role of the "velocity scale"

A feature of small scale wind models that may be unfamiliar to some readers, and is crucial for the interpretation of results given in this paper, is that such models diagnose not the actual mean winds at some point(s), but rather, *ratios* of the mean velocities to some reference value U_{REF}, a reference windspeed at some point *within, or at the boundary of, the model domain*. U_{REF} is chosen as the reference (or 'scale') on grounds of convenience, and might for example be the wind aloft at the top of the boundary layer, or possibly for models resolving only a shallower layer of the PBL, the 'friction velocity' implied by the shear stress along the top of the model domain. And if *on external grounds* (i.e. from a measurement, or as provided by some model of wider cognizance) we know or postulate a numerical value for U_{REF}, we can infer a definite value for the velocity at any other point within the model domain. A direct implication of all this for the present study, is that local windflow models can at best predict not the absolute variance of tree sway angle, but rather, how much greater is that variance at one point in the flow domain than at another.

4. Simulation of Raynor's forest-edge flow

Raynor (1971) reported mean profiles of horizontal windspeed at various distances from the upwind edge of a pine forest, during periods of flow at near-normal incidence to the forest edge. We simulated Raynor's experiment with the full model (i.e. including a full PBL, with Coriolis forces and the transverse component V) described in Section 3. Our motivation in

doing so was to determine whether the excellent simulations of Raynor's experiment given by Li et al. (1990) rested in any essential way on the closure they used, that of Li et al. (1985), described earlier – or whether the present closure would perform as well. In particular, LLM did not state whether their successful simulation of the jet observed near the base of the canopy depended on their having included their parametrization of the sweep-ejection mechanism (the term $c(U_h - U)$ in Eq. (6)), or whether the jet was an edge effect associated with low area density deep in the canopy.

4.1. Numerical details

Our computational domain for simulating Raynor's experiment extended alongwind from $x/h = -20$ to $x/h = 30$, with the forest edge at $x = 0$. The height of the domain was $40h$. Resolution was uniform at $(\Delta x/h, \Delta z/h) = (0.1, 0.1)$ over the region $x/h \leq 15$, $z/h \leq 2$; outside that region, the grid was gently stretched. Inflow profiles were obtained by solving the governing (U, V, k) equations with $\partial/\partial x = 0$, and with $c_d a h = 0$. The lengthscale was treated as adjusting instantly at the forest edge, from the open-plain profile to the forest profile ($\gamma = \infty$).

LLM adopted an approximately triangular area-density profile for Raynor's forest (their Fig. 2), but did not report the value used for their drag coefficient. Adopting essentially the same area-density profile, and treating the drag coefficient as free to be optimised, we set

$$c_d a h = (c_d a h)_0 \begin{cases} \dfrac{z/h}{0.75}, & \dfrac{z}{h} \leq 0.75 \\ \dfrac{1 - z/h}{1 - 0.75}, & \dfrac{z}{h} > 0.75 \end{cases} \qquad (20)$$

4.2. Results

A simulation using this area density profile, with $(c_d a h)_0 = 2.0$, is given on Fig. 1. The observed windspeeds, which we extracted from Raynor's Fig. 3, have been normalised on windspeed at $z = 108$ m on his 'Ace tower.' Similarly, model windspeeds were re-normalised on the inflow windspeed at that height. Agreement of our simulation with Raynor's data is good, comparable in quality with the LLM simulation. We find the occurrence of the 'jet' in the base of the canopy is dependent on specifying the reduced area-density near ground; it vanished when we set $c_d a h = \text{const}$. It follows that the heuristic source $c(U(h) - U)$ introduced by LLM in their U-momentum equation did not play a vital role in their simulation: the (simulated) jet is an edge effect in the open region at the bottom of the pine canopy.

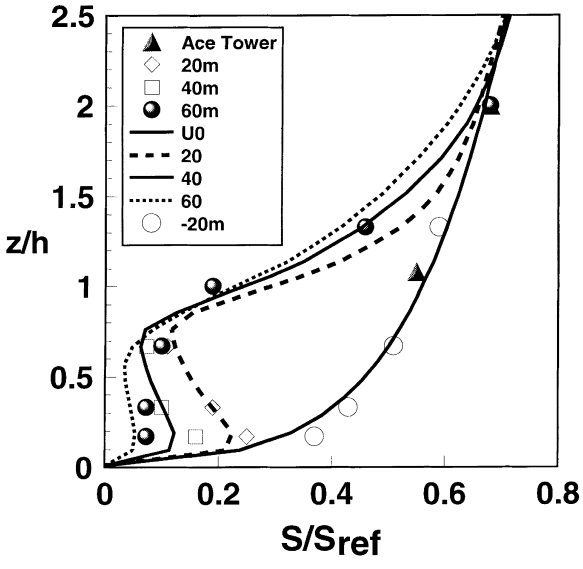

Fig. 1. Vertical profiles of mean horizontal windspeed observed by Raynor (1971) at various locations near the edge of a pine forest, in comparison with a simulation using the present model. Profile locations are given in [m] relative to the forest edge, with positive values lying *within* the forest. Note the jet deep in the canopy, simulated quite well by the model.

We did not add the simple lengthscale-interpolation used by LLM near the forest edge, nor try to equal in detail their results. In our view Fig. 1 establishes that our closure and our formulation of the lengthscale provide a simulation of Raynor's experiment that is as good as that of Li et al. (1990), while being more general in scope (e.g. use of TKE to derive velocity scale; canopy lengthscale linked to inflexion-point shear rather than leaf area density) and carrying a reduced burden of closure constants.

5. Simulation of wind-tunnel clearing-edge flow (Abbott's booby study)

In a study concerned with nesting habits of birds near forest clearings, Raupach et al. (1987) (hereafter RBG) measured mean windspeed and turbulence

statistics across clearings of widths $4.3h$ and $21.3h$ in a model canopy, within a wind tunnel. The same canopy was later used in the 'Furry Hill' experiments (Finnigan and Brunet, 1995), but some unexplained and possibly important differences are evident between the respective *equilibrium* flows (i.e. between dimensionless flow properties upstream from the clearing and from the hill). In simulating the Abbott's Booby flow we adopted the same canopy and flow parameters as did WFR for simulating Furry Hill, namely $c_d ah = 0.32$, $d/h = 0.71$.

Experimental data cited below were extracted for heights $z/h = 0.25, 0.5, 0.75, 1, 1.5$ from graphs in the RBG report. A sizeable uncertainty surrounds some of the data, where several profiles merged on the original graphs. The floor of the wind tunnel was roughened with gravel (nominal diameter, $d_g = 7$ mm) within the clearing. A rough estimate of the effective roughness length is $z_{0c} \approx d_g/10$, giving $z_{0c}/h \approx 0.015$; while at mid-clearing ($x/h = 12.8$) the mean windspeeds at $z/h = (\frac{1}{4}, \frac{1}{2})$, if plotted against $\ln_e z$, imply $z_{0c}/h = 0.001$. Simulations were not very sensitive to this parameter (clearing roughness length).

5.1. Numerical details

We dropped the *V*-momentum equation and the Coriolis term in the *U*-momentum equation, the model reducing essentially to that given by WFR, but differing in that the disturbance is here driven, not by a hill-induced pressure-gradient (WFR), but by the irregular distribution of canopy drag. Like WFR, we simulated the entire wind tunnel boundary layer, incorporating the vertical gradient in shear stress above the canopy by the imposition of an effective streamwise pressure gradient, in the present case estimated (from the observed stress gradient) as $\partial(P/\rho u_*^2)/\partial(x/h) \approx -0.23$. This step results in reproduction of the above canopy stress and TKE gradients by the model, but as WFR also found, it is not crucial for a good simulation of the streamwise changes near and within the canopy.

We simulated the flow through the wide ($21.3h$) clearing, because RGB provided more complete documentation of that case, giving profiles both within and downwind of the clearing. Our computational domain extended alongwind from $x/h = -10$ to $x/h = 40$, with the upwind edge of the clearing at $x = 0$. The domain height was $40h$. Resolution was uniform at $(\Delta x/h, \Delta z/h) = (0.2, 0.1)$ over the region $x/h \leq 21.3$, $z/h \leq 2$; outside that region, the grid was gently stretched.

As mentioned above, the Abbott's Booby profiles reported at $x/h = -2$ are somewhat unusual. Largest shear stress occurred not at $z = h$ (where normally expected in a wind tunnel boundary layer), but at $z \approx 1.5h$. Relationships between velocity statistics at that height appear normal: the maximum shear stress implied a friction velocity $u_* \approx 1.08$ (m s^{-1}); the corresponding maximum TKE[2] was approximately $k_{mx} = 6.11$ (m^2 s^{-2}), implying $k_{mx}/u_*^2 = 5.24$ ($\sigma_u/u_* = 2.11$, $\sigma_w/u_* = 1.25$), which is close to the value observed upstream from Furry Hill, $k(h)/u_*^2 = 5.6$. However at $z = h$, TKE appears to be anomalously small, with $k(h)/U^2(h) = 0.25$, whereas the corresponding value for the equilibrium flow upwind from Furry Hill was $k(h)/U^2(h) = 0.37$.

5.2. Results

For the comparisons to follow we renormalised observed and modelled (U,k) on a velocity scale (U_{ref}) chosen as the velocity (observed/modelled) at $(x/h, z/h) = (-2.1, 1)$: i.e. $U_{ref} = U(-2.1,1)$. The lengthscale adjustment parameter $\gamma = 0.05$ for the results shown. Fig. 2(a) compares the observed and modelled mean winds across the clearing in the form of a set of horizontal profiles, while Fig. 2(b) gives vertical profiles. The normalised profile of mean windspeed observed by RBG upwind from their clearing closely matches that observed by Finnigan and Brunet upwind from Furry Hill (first panel of Fig. 2(b)), and as we use the same canopy parameters as did WFR, we obtain the same (excellent) model equilibrium profile, characterised by $U(h)/u_{*0} = 3.76$, where u_{*0} is the friction velocity based on shear stress at $z = h$.

At the highest level ($z/h = 1.5$) the simulation overestimates velocity at all stations, including the 'inflow' station at $x/h = -2.13$. This may indicate an inconsistency between the model assumption of an infinite upwind extent of uniform canopy, and the actuality of the experiment. Otherwise the general response of the windspeeds across the clearing and back into the canopy is modelled quite well, except that in the middle of the clearing ($x/h = 12.8$) speeds have been

[2] (σ_v was not measured: we assumed $\sigma_v = \sigma_w$).

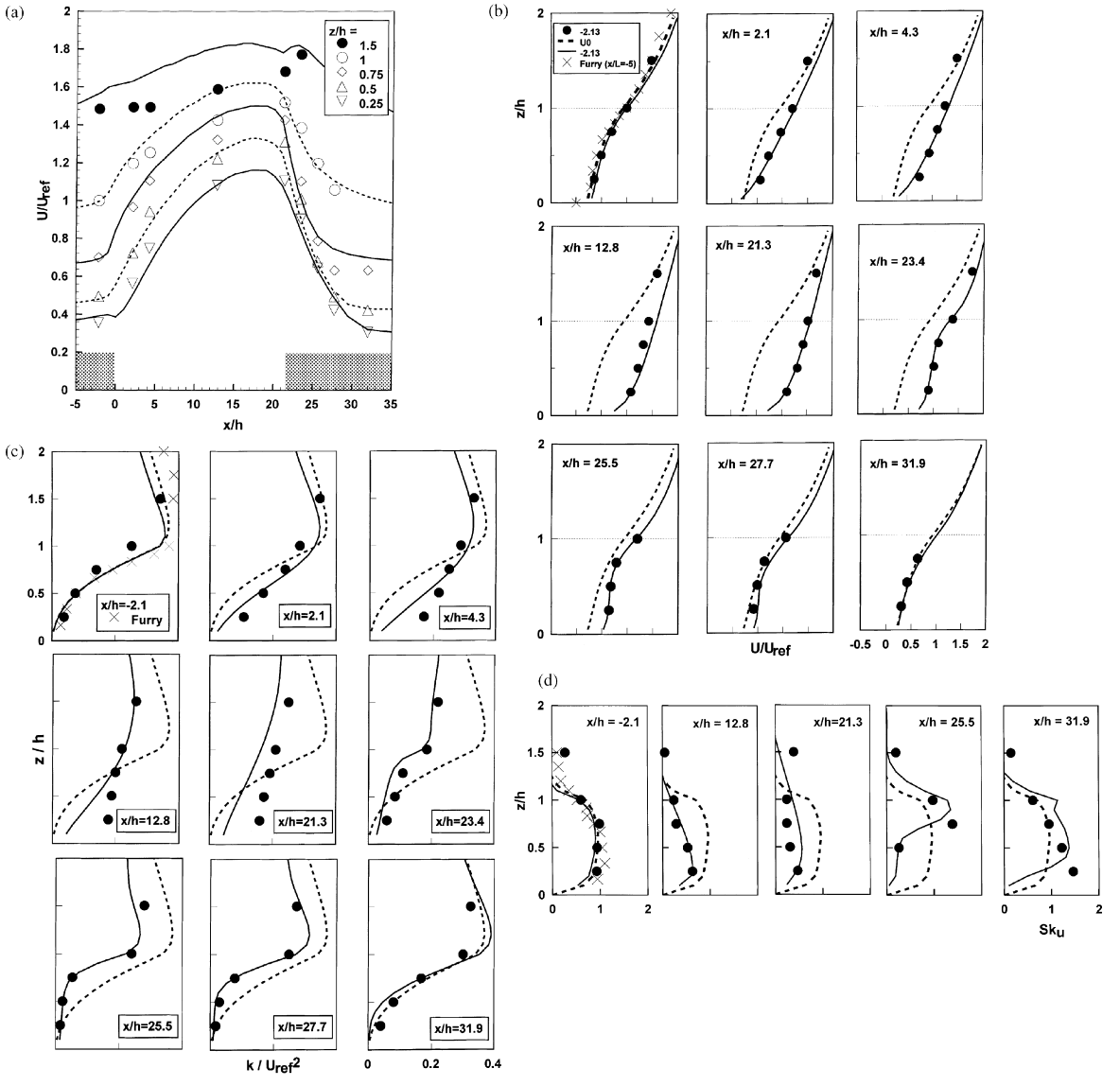

Fig. 2. (a) Horizontal profiles of the normalised mean windspeed across a clearing in a model forest: comparison of observations (symbols) from the 'Abbott's Booby' study with numerical simulation (lines). U_{ref} is the velocity at $(x/h, z/h) = (-2.13, 1)$. (b) Sequence of observed (●) and modelled (solid line) vertical profiles of the mean windspeed across the Abbott's Booby clearing, which spanned $0 \leq x/h \leq 21.3$. The heavy dashed line on each panel gives the *equilibrium* model solution as a reference for the alongwind changes in windspeed. The first panel also shows the wind profile observed within the same canopy, in subsequent experiments by Finnigan and Brunet (1995), far upwind from Furry Hill. (c) Sequence of observed (●) and modelled (solid line) vertical profiles of normalised turbulent kinetic energy, k/U_{ref}^2, across the Abbott's Booby clearing. The heavy dashed line on each panel gives the *equilibrium* model solution as a reference for the alongwind changes. The reference windspeed $U_{\mathrm{ref}} = U(-2.13, 1)$, and had observed value 4.22 (m s^{-1}). Also shown (×) is the profile of k/U_{ref}^2 observed in the same canopy, far upwind from Furry Hill, where $U_{\mathrm{ref}} = 3.60$ (m s^{-1}). Observed values of k/U_{ref}^2 at $z = h$ were (0.25, 0.37) upwind of the clearing and upwind from Furry Hill, while $k/U_{\mathrm{ref}}^2 = 0.32$ for the model equilibrium profile. (d). Sequence of observed (●) and modelled (solid line) vertical profiles of the alongwind velocity skewness Sk_u across the Abbott's Booby clearing. The model skewness is the solution of Eq. (A2). The heavy dashed line, repeated on each panel, serves as a reference for the alongwind changes: it gives the *equilibrium* skewness for uniform flow in this canopy, and was calculated using Eq. (A3) with $\kappa = 1$ for the model's equilibrium profiles of shear stress, TKE, and TKE dissipation rate. Also shown (×) on the first panel is the profile of Sk_u observed in the same canopy, far upwind from Furry Hill.

overestimated. The observed data at that station are not subject to doubt, as least as regards their extraction by us off the RBG report, and we have no explanation as to why the adjustment of the clearing flow is modelled well everywhere but in this neighbourhood. Incidentally, the simulations were for all practical purposes insensitive to the manner of lengthscale blending near the forest wall, so that there is no justification (in this case) for anything more complex than immediate adjustment from the forest- to open-plain forms for the lengthscale.

Fig. 2(c) compares simulated and observed vertical profiles of TKE from the Abbott's Booby experiment. Regarding the upwind profile, we have already mentioned that observed TKE at $z = h$ is surprisingly small, $k(h)/U^2(h) = 0.25$ (cf. 0.37 for the Furry experiments with the same canopy in the same tunnel). This could be regarded as consistent with the reported shear stress profile for that location (not shown here), which places the most-negative shear stress not at $z/h = 1$, but at about $z/h = 1.5$. Just as a *positive* stress gradient (i.e. magnitude of the shear stress decaying with increasing height) above $z = h$ implies $\partial k/\partial z < 0$ in that region (e.g., as seen far upwind from Furry Hill), the *negative* stress gradient above $z = h$ seen here can be taken as implying increasing shear-production of TKE – raising the height at which peak TKE occurs. These aspects of the observations could easily be reproduced in simulations, by incorporating a shallow region of *adverse* background pressure gradient below $z/h = 1.5$, and resulted in essentially perfect simulation of the TKE profile at $x/h = -2$. However that modification of the background pressure did not substantially alter predicted TKE at downwind stations (other than near z/h=1.5). Therefore because this interpretation of a 'back pressure' layer is entirely speculative, and the cause for it (if true) unknown, we have presented simulations without it.

Variation of the TKE across the Abbott's Booby clearing resembled that observed in a wider wind tunnel clearing by Chen et al. (1995) (hereafter CBNA). Our simulation at least reproduces the dominant features, a transition near ground from low TKE deep in the canopy toward larger values characteristic of open ground, with concomitant decrease of TKE aloft (smoother surface), and rapid development of a strong vertical gradient near $z = h$, upon transition back into the canopy. Interestingly, the model equilibrium TKE-profile matches the observations farthest *downwind* ($10.6h$) from the clearing ($x/h = 31.9$) somewhat better than the observations upwind (we have already expressed some uncertainty about that upwind TKE profile). Nevertheless as the local solution at $x/h = 31.9$ differs from equilibrium, one cannot regard those observations as representing equilibrium.

Our modelled TKE was not appreciably improved by setting $\mu = 1$ within the clearing (as usually recommended for an equilibrium wall shear layer flow) to increase downward transport of TKE, nor by altering the surface boundary condition on TKE to increase k_{gnd} (by writing $k_{\mathrm{gnd}} = \beta u_*^2/c_\varepsilon$, with $\beta > 1$). Liu et al. (1996) reported comparably successful simulation of the CBNA clearing flow, provided they re-tuned the standard k–ε model, without which step discrepancies of order 100% relative to the observations occurred (their Fig. 9).

A very interesting aspect of the Abbott's Booby study was the identification of a region of very high velocity skewness just within the forest at the leeward edge of the clearing, believed to explain the birds' avoidance of such locations as nesting sites. Fig. 2(d) compares modelled and observed skewness profiles. The equilibrium skewness profile is diagnosed rather well (except for the point at $z/h = 1.5$, which is remedied if one includes the adverse-pressure layer), as is the decrease in skewness within the clearing, and the prompt re-development of large skewness, building down from z/h, at the downwind edge of the clearing.

As mentioned earlier, simulations of the Abbot's Booby experiment with $\gamma = \infty$ (instantaneous adjustment of the lengthscale to the infinite-plain formulation upon passage into a clearing) were quite as satisfactory as any other choice. This insensitivity to the precise manner in which the lengthscale is adjusted at the forest boundaries suggests that, in the region of those boundaries, diffusion terms in the momentum and TKE budgets are of lesser importance than other terms, such as advection and the pressure-gradient force.

6. Simulation of periodic forest cutblocks (Manning, Alberta)

We now arrive at the issue motivating this paper: can a flow model sufficiently well diagnose wind and

turbulence within forest cutblocks as to provide (via the wind statistics/tree sway connection established by Flesch and Wilson, 1999b) a useful indication of implied (remnant) tree sway – an issue to be tested by comparison of our model, which we have argued is as well-tested and as successful as any earlier effort to describe flow in irregular forests, against observations in the Manning cutblocks.

As those data stem from very windy intervals, we shall not be concerned with any influence of thermal stratification upon the flow. We have no measurements whatsoever on the basis of which to diagnose the depth of mixing, and the winds aloft. Therefore although the simulations we present carry a full PBL, the aim was not to replicate the actual (unknown) details of the flow aloft, but merely to ensure that the modelling of the disturbed flow through the cutblocks was not compromised by an inherently unrealistic treatment aloft.

6.1. Numerical details

One-dimensional solutions for U,V,k, representing an infinite forest block, were imposed at $x/h = -80$. A forest block covered $-80 \leq x/h < -60$; a large 'reference clearing' spanned $-60 \leq x/h < -30$, within which the model's 'reference anemometer' lay at $x/h = -40$; and another forest block covered $-30 \leq x/h < 0$. At the model origin $x = 0$ lay the upstream edge of the first of a sequence of three (narrow) or four (wide) cutblocks, of widths X_c^i $(i = 1, 2 \ldots)$, and each terminated by a forest strip of equal or comparable width (X_f^i); specifically, for the ''narrow'' clearings, $(X_c^i = 1.7$ h; $X_f^i = 2.3$ h; i=1,2,3); while for the ''wide'' clearings, $(X_c^i = X_f^i = 6.1$ h; i=1,2,3,4). The leeward-most of these clearings represented our instrumented cutblock. At $x > \sum_i (X_c^i + X_F^i)$ a forest block extended downstream to the outflow boundary at $x = +96h$, where we imposed $\partial_x(U, V, k) = W = 0$.

Alongwind resolution was uniform ($\Delta x/h = 0.1$ for the $1.7h$ simulations; $\Delta x/h = 0.2$ for the $6.1h$ case) between $x/h = -70$ (which point lay upwind from the reference clearing) and a point lying well downstream of the final (i.e. test) cutblock. Further towards either end of the domain, the grid was stretched. Below $z = 2h$, vertical resolution was $0.09h$, while above, the grid was stretched.

For simplicity, and as we lacked measurements to guide any more complex choice, we used constant values for a and c_d: we treated γ and the bulk dimensionless parameter $c_d ah$ as free to be optimised (see Section 6.3.4).

6.2. Rescaling model output to compare with observations

The field experiments at Manning mismatch the model in that slight irregularity in forest cover and topography occurred upstream from the windward $(i = 1)$ cutblocks. Our choice of the (unknown) Geostrophic velocity component U_G as velocity scale for the model was simply a convenience. To compare model output with our data, we re-scaled observed and calculated velocity statistics. We shall show observations scaled on cup-windspeed ('S_{clr}') observed at $z = 9$ m in the large reference clearing, which lay some kilometers from our trial cutblocks. Model velocities were correspondingly re-scaled on the predicted (internal) value for the 9 m windspeed in the (model's) reference clearing.

6.3. Results

In the figures to follow, the coordinate x^*/h represents alongwind location relative to the upstream edge $(x^* = 0)$ of the instrumented cutblock. For all simulations to be shown, i.e. both for the $1.7h$ and the $6.1h$ clearings, unless otherwise stated $c_d ah = \frac{3}{4}$, $\gamma = 0.05$. Better concordance of the model with the data could have been had by permitting these parameters to differ between the two geometries, with the justification that there may indeed have been differences. But we felt it a more convincing demonstration of model skill that we should change *nothing* across simulations for the cutblocks of differing X_c/h. We reason in Section 6.3.4 that the choice $c_d ah = \frac{3}{4}$ provides the best overall outcome, considering both mean wind speed (S) and, more importantly as regards tree motion, turbulent kinetic energy.

6.3.1. Inflow profiles

Fig. 3 gives equilibrium profiles, for the case $(U_G = 1, V_G = -1)$, of wind velocities $U_0(z)$, $V_0(z)$, the cup windspeed $S_0(z) = [U_0^2 + V_0^2]^{1/2}$, shear stress τ_0, turbulent kinetic energy k_0 and mean wind direction. We have (here only) re-normalised relative to the canopy-top friction velocity $u_{*0} = [\langle u'w' \rangle^2 + \langle v'w' \rangle^2]^{1/4}$,

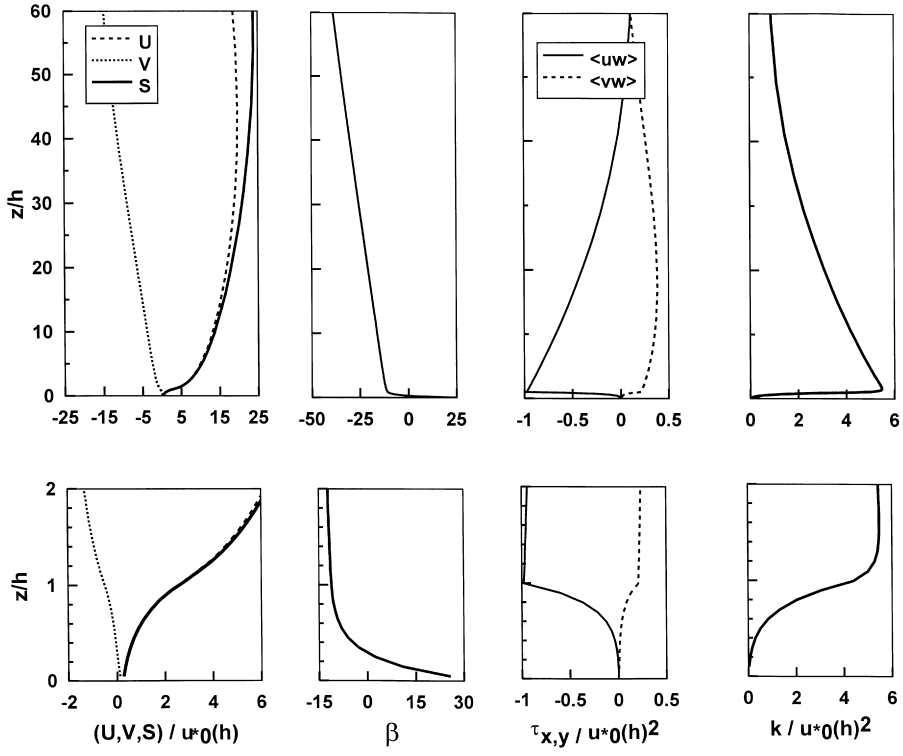

Fig. 3. Equilibrium profiles of horizontal velocity components, cup windspeed (S) and mean wind direction (β), shear stress (τ) and turbulent kinetic energy (k), these being the inflow profiles for simulations of the Manning cutblock flows.

to permit easy comparison with other such forest profiles (u_{*0} being the velocity scale usually preferred); our ratio $S_0(h)/u_{*0} = 2.7$, a value which is fairly typical of a dense canopy. The profiles of Fig. 3 constitute the inflow boundary condition, towards which the flow reverts on each re-entry into forest.

We were surprised by the large swing in wind direction across the canopy ($0 \leq z/h \leq 1$), which is as large as the swing across the entire upper domain $1 \leq z/h \leq 80$. An organised swing of mean wind direction within the canopy, induced by the rapidly-decreasing Coriolis force in a region of very low windspeed and resulting in alignment of the velocity with the pressure-gradient force, makes obvious sense. But it has not been widely apprehended in observational studies, perhaps because the database of wind observations within canopies is substantially derived from cup anemometers, and from wind tunnel studies. An implication is that, even in disturbed flows having two-dimensional symmetry, such as those of our cutblock records when the winds (at observation level) blew nearly perpendicularly across the forest borders, disturbances in wind direction may be anticipated. Of course, such Coriolis-force-related changes may well be masked by imperfections in the crosswind symmetry (gaps in the forest, or irregularities in the edgeline), and other departures of the flow from the ideal envisaged in the model. In any case, given this strong height-dependence of equilibrium wind direction, we are forced to accept that a full-scale forest-clearing flow which is at all heights perpendicular to the forest edges is unrealisable, i.e. dynamically disallowed, except where it occurs in response to some fortuitous conspiracy of upwind topography, etc. The best we can hope for is a near-ground flow that is *roughly* perpendicular to the forest edges; our specification ($U_G = 1$, $V_G = -1$) results in the mean wind direction lying only 6° away from the x-axis, at (the model's equivalent of) the position of the anemometer in the 'reference clearing.'

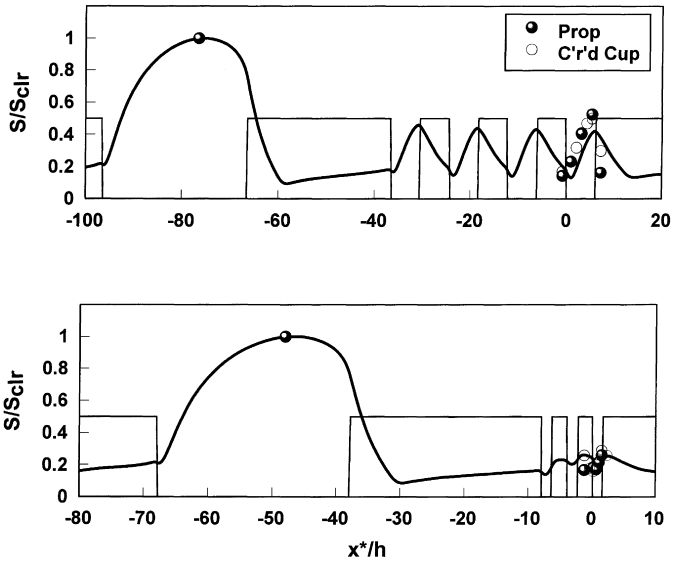

Fig. 4. 'Grand scale' comparison of measured and simulated spatial variation of the normalised mean cup windspeed S/S_{clr}, at $z = 9$ m, across the reference clearing and through the periodic arrays into the instrumented cutblocks. Simulation assumes $c_{\mathrm{d}}ah = \frac{3}{4}$, $\gamma = 0.05$. Range on the x^* axis covers of order 5 km, and $x^* = 0$ at the upwind edge of the instrumented cutblock. Observations consist of all propellor data for $|\beta| < 30^\circ$, all cup data for $|\beta| < 10^\circ$.

6.3.2. Mean windspeed and pressure

Fig. 4 compares the modelled and measured patterns of variation in the mean cup-windspeed $S(x, z_{\mathrm{instr}})$ through the reference clearing and far downwind across the cutblock arrays. Similar patterns hold for the U component, because we assured $V \ll U$ at $z = 9$ m by specification of V_{G}. Model and experimental data have been re-normalised on S_{clr}, which assures their agreement (that $S/S_{\mathrm{clr}} = 1$) at instrument height ($z = z_{\mathrm{instr}} = 9$ m) at the distant reference point. So that anyone who wishes to may (again) re-normalise our model fields on u_{*0} (friction velocity based on the shear stress at $z = h$ of the equilibrium, i.e. inflow, profiles) we note that in our simulations $S_{\mathrm{clr}}/u_{*0} = 3.83$.

It is apparent from Fig. 4 that the model calculates nicely the overall wind reduction in the cutblocks, relative to S_{clr}, which can be regarded essentially as a weather-station (open ground) reference. For the $6.1h$ cutblocks there is little variation from one cutblock to the next in the amplitude of the wind-modulation, and even the peaks differ only modestly from one cutblock to the next. This is consistent with findings of Raupach et al. (1987) for a clearing within a wind-tunnel model canopy. It follows that our instrumented cutblocks, at least in the $6.1h$ array, should have been 'typical' of their neighbours, and that a periodic boundary-condition might be used to model the flow in a single representative cutblock. Simulations of the $6.1h$ experiment, using a three-dimensional generalisation of the present model that assumes periodicity on the x and y axes, agree closely with those presented here (A. Tuzet, pers. comm). Apparently however, windspeed may not have been periodic across the narrower, $1.7h$ cutblock array.

Although good overall conformance of model and observation is apparent on Fig. 4, on taking a close-up view (Fig. 5) one observes that the amplitude of the variation of S/S_{clr} across the $1.7h$ cutblocks has been underestimated, and that in the $6.1h$ cutblock, the 'wave' of S/S_{clr} seems slightly out of phase with the observations (the latter feature would vanish upon scaling on an in-cutblock reference windspeed S_{cb}, and so may be only a consequence of imperfect simulation of $S_{\mathrm{clr}}/S_{\mathrm{cb}}$ by the model). In assessing Fig. 5 one should bear in mind several mitigating points. Firstly, we have little confidence in our within-forest wind data. The forest blocks were quite inhomogeneous as regards tree height, spacing, and species-mix, and so a point measurement need not

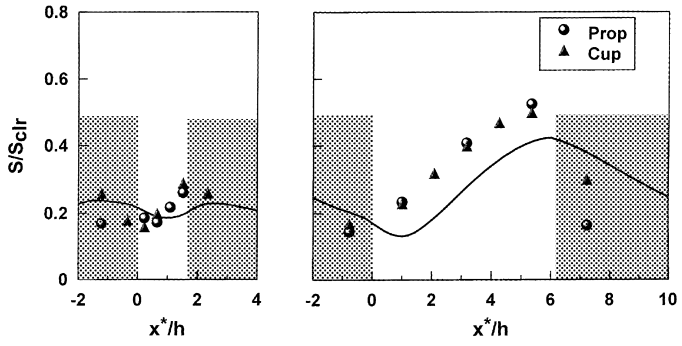

Fig. 5. 'Local view' of measured and simulated spatial variation of the normalised mean cup windspeed $\boldsymbol{S}/\boldsymbol{S}_{\mathrm{clr}}$, at $z = 9$ m, across the instrumented cutblocks. Simulation assumes $c_{\mathrm{d}}ah = \frac{3}{4}$, $\gamma = 0.05$. Observations consist of all propellor data for $|\beta| < 30^{\circ}$, all cup data for $|\beta| < 10^{\circ}$.

compare well with the model's implicitly spatially-averaged figure. Secondly, we have entirely neglected the topographic variations of the terrain, and the drag of the remnant trees in the cutblocks. Thirdly, we have used the same, constant value for $c_{\mathrm{d}}ah$ across the entire domain (except in clearings, where $c_{\mathrm{d}}ah = 0$), whereas undoubtedly in-forest spatial variations in $c_{\mathrm{d}}ah$ occurred. We did not feel it was warranted to 'guess' our way about by adjusting a spatially-varying $c_{\mathrm{d}}ah$, an approach which would amount to no more than an exercise in curve-fitting. Finally, perhaps most significantly of all as regards the apparently flawed model performance (Fig. 5), the field reference windspeed S_{clr} was measured in a clearing about 5 km from our instrumented cutblocks, and separated from them by rather irregular terrain, whereas the model reference clearing lay immediately upwind of the cutblock array. Thus it would be naive to expect of the model a perfect profile of S/S_{clr}, and one might with some justification contend it would be fairer to assess model skill with respect to properties scaled on a *local* velocity scale (measured *in* the test cutblock); see Wilson and Flesch (1996), who gave model output in such form.

Our measurements provided no information on the vertical variation of the wind patterns throughout the cutblocks. Fig. 6 gives an alongwind sequence of modelled vertical profiles of the U component, across the $X_{\mathrm{C}} = 6.1h$ cutblock. An initially surprising feature is that, below about $z/h = \frac{1}{2}$, the alongwind compo-

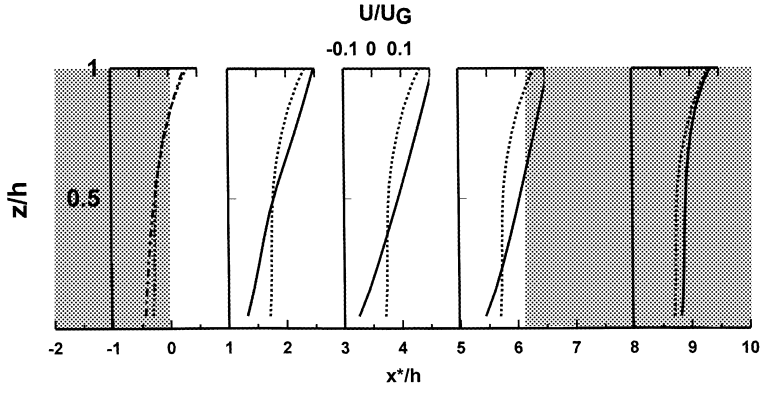

Fig. 6. Vertical profiles of the alongwind velocity component U/U_{G}, at several locations across the $X_{\mathrm{F}} = X_{\mathrm{C}} = 6.1$ h cutblock. The span of the velocity axes is $(-0.1, +0.2)$ U_{G}, and the height-axes are placed so as to mark the locations (in x^*/h) of the profiles. (Chain line), the equilibrium solution (infinite fetch of forest); (Dotted line), the solution at $x^*/h = -1$, i.e. just upwind of the forest → cutblock transition; and (Solid line), the local solution.

nent *U accelerates* across the forest belts and *decelerates* in the clearing, to the degree of reversal ($U < 0$) very near ground. The opposite behaviour is seen at larger heights. Unfortunately we do not have observations to confirm this complex pattern. But we feel it is plausible, in view of the reversing pressure gradients the flow encounters (more on this below).

Towards the middle of the wide clearing(s), a boundary-layer type profile is established, i.e. there is not the inflexion point characteristic of a canopy wind profile. But upon passage back into a forest block, the characteristic canopy wind profile develops promptly, with acceleration of the flow very near ground, and deceleration higher up. At the downwind edge of the forest strip (see the profile at $x^*/h = -1$), the wind profile resembles the equilibrium profile, i.e. the profile which would be observed within a forest of infinite extent (and which was used as the inflow boundary condition). More or less the same features are diagnosed by the simulations for the narrow cutblocks, with the exception that a boundary-layer type profile is not established.

In undisturbed micrometeorological flow the mean vertical velocity is of the order of a few cm/s. However sizeable vertical motion can be expected near forest edges. Fig. 7 gives contours of the normalised mean vertical velocity W/S_{clr} in the wide cutblock. Upward flow occurs within a distance of about $2h$ from the sheltering forest edge, beyond which there is descent over most of the cutblock, and even in the inflow region of the downstream forest block. Although these

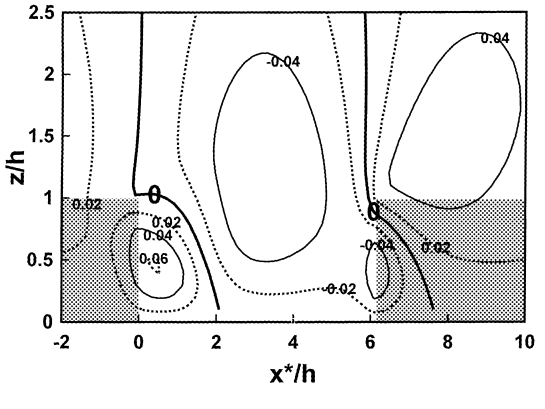

Fig. 7. Contours of mean vertical velocity W/S_{clr} in the wide clearing.

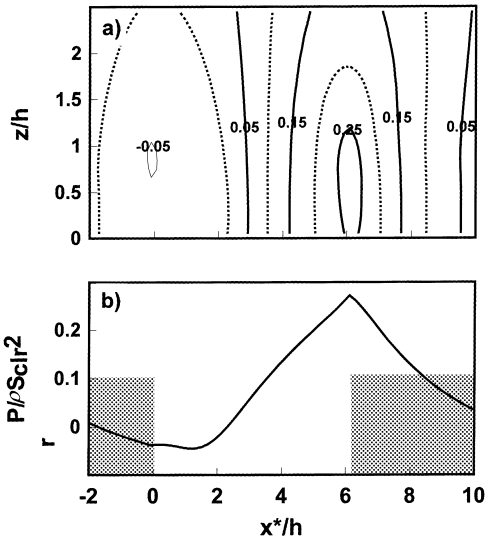

Fig. 8. Normalised pressure field $P/\rho S_{\mathrm{clr}}^2$ about the wide (6.1 h) cutblock, according to the numerical model; (a) contours; and (b) horizontal profile at $z/h = 0.4$. Pressure is not necessarily positive, being *relative* to ground-level pressure at the outflow boundary.

vertical velocities are small relative to the horizontal winds, peaking at about $0.06S_{\mathrm{clr}}$, the implied dimensional mean velocity can be large, around 0.5 m s^{-1} when $S_{\mathrm{clr}} = 10$ m s^{-1}, and is likely to have dynamical importance.

Fig. 8 gives the local pressure field about the $6.1h$ clearings. A steeply adverse pressure gradient $\partial_x P$ upwind from the clearing → forest transition gives way within the forest block to a strongly favourable (accelerating) gradient. Deep within dense vegetation, the wind is only weakly coupled to the flow aloft, and thus essentially driven by a balance between form drag and the local pressure gradient. The favourable pressure gradient across the sheltering forest belts, clearly shown in Fig. 8, presumably causes the accelerating windspeed seen near ground, while the adverse gradient in the clearing may explain the near-ground velocity-reversal.

6.3.3. Turbulent kinetic energy

Fig. 9 gives a wide-area view of our simulation of the normalised turbulent kinetic energy k/S_{clr^2}, in comparison with the observations. The simulation captures nicely the overall patterns, and Fig. 10 confirms that even the local detail is represented fairly well: the general *shape* of the modelled TKE profile

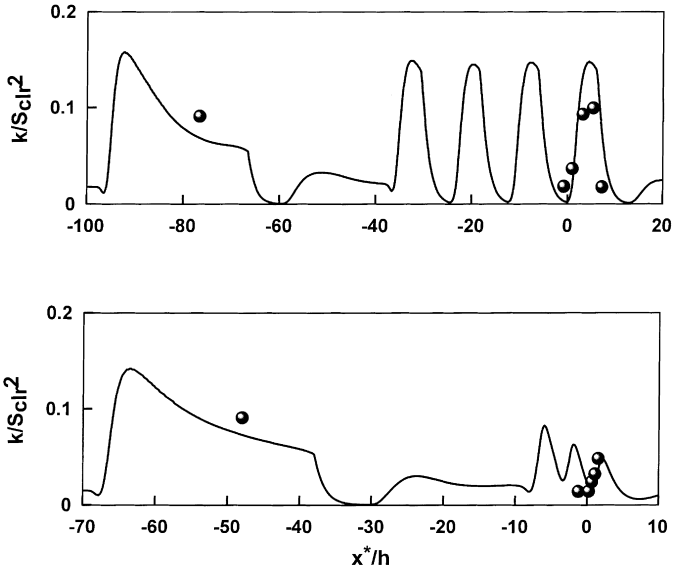

Fig. 9. Grand scale comparison of measured and simulated spatial variation of the normalised turbulent kinetic energy $\boldsymbol{k}/\boldsymbol{S}_{\mathrm{clr}}^2$, at $z = 9$ m, across the reference clearing and through the periodic arrays into the instrumented cutblocks. Simulation assumes $c_{\mathrm{d}}ah = \frac{3}{4}$, $\gamma = 0.05$. Range on the x^* axis covers of order 5 km, and $x^* = 0$ at the upwind edge of the instrumented cutblock.

matches that observed, with TKE increasing sharply over the upwind half of the $6.1h$ cutblock, and changing much less over the downwind half. In view of the provisos earlier expressed (instrument performance; neglect of terrain complexity; etc.), the modelled pattern of TKE is satisfactory, and we may infer from it the spatial variation of the velocity variance σ_u^2.

6.3.4. Weak sensitivity to lengthscale adjustment parameter γ

Fig. 11 illustrates the rather modest sensitivity of these simulations to specification of the lengthscale adjustment parameter γ; entirely different formulations of the lengthscale transition (between equilibrium forest form λ_{F} and equilibrium open plain

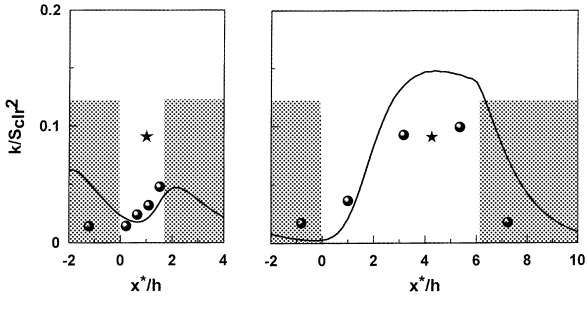

Fig. 10. Local view of measured and simulated spatial variation of the normalised turbulent kinetic energy k/S_{clr}^2, at $z = 9$ m, across the instrumented cutblocks. The simulation assumes $c_{\mathrm{d}}ah = \frac{3}{4}$, $\gamma = 0.05$. Also plotted (★) on both graphs, though not at the proper point (which lies offscale) on the x^*/h axis, is the measured value of $\boldsymbol{k}/\boldsymbol{S}_{\mathrm{clr}}^2$ in the distant reference clearing. Thus, towards the leeward region of the wide cutblock, TKE exceeds somewhat its value in that much wider, reference clearing.

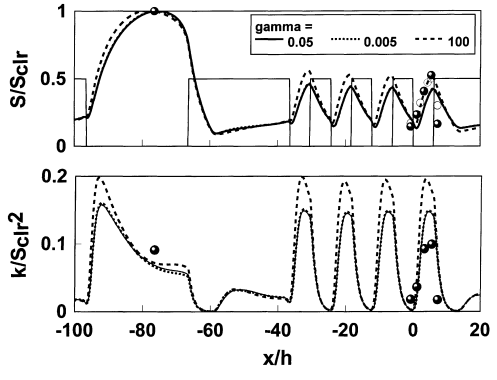

Fig. 11. Sensitivity of simulations of cup windspeed (S) and turbulent kinetic energy (k) across the wide ($6.1h$) cutblocks, to specification of the lengthscale adjustment parameter γ. The bulk drag coefficient $c_{\mathrm{d}}ah = \frac{3}{4}$ for all curves. The observations (as on Figs. 5 and 9) are also shown for comparison.

form λ_P as the asymptotic downwind limit in a large clearing) gave simulations which were equally acceptable. Variation of γ (or of the transition-formulation) has a greater impact on the TKE field than on the mean windspeed field. Although Fig. 11 shows that the choice $\gamma = 100$ provides a much better simulation of the mean wind than the $\gamma = 0.05$ we settled on, the spatial modulation of the associated TKE field is seriously overestimated. Recall that the rms wind force $\sigma_{u|u|}$, whose specification is the goal of this investigation, is considerably more sensitive to TKE than to mean windspeed (Appendix A).

There is one other 'free' parameter, $c_d ah$: should we reduce this, we reduce the modulation of both S and k. However the consequence of that step is that the variation of S across the narrow cutblock, already underestimated (Fig. 5) with $c_d ah = \frac{3}{4}$, is further reduced. Our specification that $c_d ah = \frac{3}{4}$, $\gamma = 0.05$ therefore represents a compromise, and as we shall later show, a good one as regards the resulting simulations of the rms wind force $\sigma_{u|u|}$. We do not hold that this choice is *uniquely* optimal, and the outcome is not very different for γ in the range $0.005 \leq \gamma \leq 0.5$.

6.3.5. Skewness Sk_u

Fig. 12 compares the average pattern of skewness observed, with solutions of the simplified Sk_u budget equation given in Appendix C. We observed large run to run variability in Sk_u, which cannot be explained within the scope of a 2-d flow model. This variability probably arose from our short averaging intervals (15 or 30 min), and perhaps partly from imperfect response of the propellor anemometers. The simulation of Sk_u is disappointing, in view of the encouraging result we reported for the Abbot's Booby clearing. Fortunately, however, the variance $\sigma^2_{u|u|}$ of the wind force is much less sensitive to Sk_u than to the lower moments.

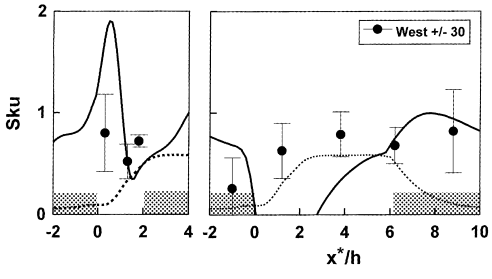

Fig. 12. Observed versus modelled Eq. (A2) horizontal profiles of velocity skewness Sk_u at $z = 9$ m. The dashed line results from having dropped the production term $3\alpha^2_{sk} k \partial_x k$, which otherwise (solid line) causes large negative Sk_u near the upwind edge of the wide clearings.

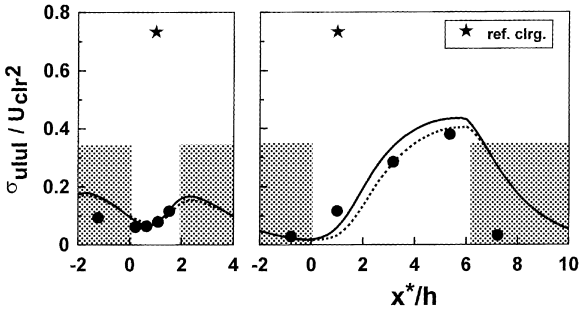

Fig. 13. Comparison of measured and modelled spatial variation of the normalised wind force $\sigma_{u|u|}/U^2_{clr}$ across the instrumented cutblocks and in the distant reference clearing (★, actually observed far upwind on the x^*/h axis). Simulation assumes $c_d ah = \frac{3}{4}$, $\gamma = 0.05$. For the calculation of $\sigma_{u|u|}$ according to Eq. (1), we assumed $Kt_u = 4$ and either set $Sk_u = 1$ (solid line), or calculated Sk_u according to Appendix C (dashed line). Note that $\sigma_{u|u|}$ determines the standard deviation of tree sway angle σ_θ, and that U_{clr}, being measured in a large clearing, can be considered as more or less a weather station windspeed.

6.3.6. Wind force $\sigma_{u|u|}$ and tree sway

Fig. 13 compares the observed spatial pattern of the normalised wind force $\sigma_{u|u|}/U^2_{clr}$ against the simulations. The velocity variance σ^2_u was derived from the calculated TKE, assuming equilibrium partitioning, i.e. $\sigma^2_u = c_e c^2_u k$. We set kurtosis $Kt_u = 4$ (a value typical of our measurements), and as anticipated (Appendix A) found the modelled wind force was not very sensitive to the specification of skewness Sk_u, witness the small difference between the outcome using $Sk_u = 1$ and that using model-calculated skewness.

The model has captured very well the dramatic reduction of the wind forcing relative to the distant reference clearing, and has given quite precisely the local detail of the pattern of wind force within the cutblocks. Given the tight connection between $\sigma_{u|u|}$ and tree sway, we are now in the position that, once given a figure for U_{clr}, which is more or less a 'weather station' windspeed, we may infer the r.m.s. sway σ_θ of a 'characteristic' (remnant spruce) tree, whatever its position in the array of cutblocks.

7. Model investigation of the effect of forest border width

As an example of the potential of a windflow model to evaluate strategies for minimising windthrow, we shall investigate the consequence of using forest strips of *reduced width*, $X_F = 3h$ or $X_F = 1h$, to shelter remnant spruce in cutblocks of unaltered width $X_c = 6.1h$.

The sole difference between the simulations required for these three cases ($X_F/h = 6.1$, 3, 1) is the distribution of forest-drag. We made no changes to the grid distribution, to the location of the large upstream 'reference clearing' wherein the velocity scale S_{clr} is 'measured,' nor to the input parameters ($c_d ah = \frac{3}{4}$, $\gamma = 0.05$). As previously, we focus on the wind properties in the downwind member of a *series* of four cutblocks, each of which is *equally* provided with a shelter-strip (of width $X_F/h = 1$, 3, or 6.1).

Fig. 14 shows the comparative profiles of speed, TKE and rms wind-force within the 'test' cutblock (width $6.1h$), as provided with either a $1h$, a $3h$, or a $6.1h$ shelter-block. According to the model, if $3h$ shelter blocks are provided (rather than $6h$ blocks), mean windspeed reduction is not so favourable, though still entirely acceptable ($S < 0.4\ S_{clr}$); while, quite unexpectedly, the TKE is *greatly* reduced over much of the cutblock, falling to about as low as only 25% of the *already* reduced TKE figure when 6h shelter was provided! The consequence is that wind protection is *markedly better* when the shelter strips are only $3h$ wide than when they are $6.1h$ wide.

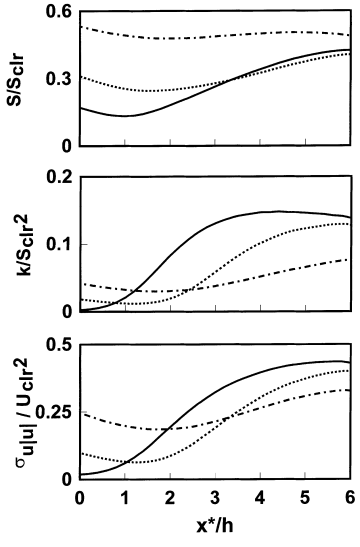

Fig. 14. Comparative numerical simulations of the patterns of windspeed (S), turbulent kinetic energy (k) and root-mean-square wind force ($\sigma_{u|u|}$) across the fourth of a series of cutblocks, each having width $X_c = 6.1h$, and each sheltered by forest strips of width $X_F = 6.1$ h (solid line), $X_F = 3h$ (dashed line), or $X_F = h$ (dot-dashed line). Simulations with $c_d ah = \frac{3}{4}$, $\gamma = 0.05$.

Whether or not this is true, only comparative observations can decide. In the first paper of this series, we summarised observations of TKE across a number of clearings from different experiments, and found a striking uniformity in the pattern of TKE 'recovery.' The present simulations (of clearings with forest borders of $X_F = 3h$ or $X_F = 1h$) do not uphold the pattern: in both cases they show an initial *decrease* in TKE with increasing x across the clearing. Perhaps the explanation for this discrepancy lies in the fact that none of the experimental clearings had a geometry like that we have simulated. In any case, if the predictions of Fig. 14 should prove to be in conflict with observation, one would be impelled to conclude that the earlier-shown concordance of the model with observations (see Sections 4–6) is largely spurious, perhaps only the fortuitous consequence of 'tuning.' That possibility is scarcely believable, we think: for example, there simply *was* no tuning in the case of our simulation of the Abbott's Booby study.

Well, if this unexpected model result were true in reality, then why? Why would *narrower* shelter strips provide *more effective* reduction of the r.m.s. wind force? In contemplating the matter, recall that the impact of the shelter on *turbulence* is more important than its impact on the mean wind. Although the influence of porous-shelterbelt thickness (W) on *mean* wind reduction has been studied computationally (Wang and Takle, 1996) and experimentally (Takahashi, 1978), and whilst others have investigated the influence of *spacing* of successive porous barriers (screens, $W \approx 0$; or thick windbreaks of various W) on *mean* wind, we are not aware of any existing comprehensive study of the pattern of *TKE* around a sequence of porous barriers of arbitrary width (W) and spacing. In interpreting Fig. 14, then, we can only speculate. The act of providing shelter in one region so as to reduce near-ground windspeed *causes* a downwind region of increased vertical shear, and associated

turbulence (increased shear production in Eq. (12): and so perhaps the provision of *wider* forest strips leads to stronger vertical wind shear at the upwind edge of the protected zone (cutblock) than does provision of narrower shelter, causing accentuated shear production of turbulence, and the surprising r.m.s. wind-force pattern suggested by Fig. 14.

8. Conclusions

Our aim has been to combine a high-resolution (order 1 m) wind and turbulence model, with a tree-motion model, to infer statistics of remnant tree sway in forest clearings. To that end we have adapted the K-theory closure of Wilson et al., (1998; WFR), tested it against our own and others' observations of forest-edge flows, and showed it performs at least as well as the more-complex models of earlier authors. With appropriate choices of domain size, resolution, etc., simulations show quite good agreement with observations of mean windspeed and turbulent kinetic energy, without alteration of the basic closure parameters (c, α, μ) formerly optimised by WFR. The implied spatial patterns of the root-mean-square wind force $\sigma_{u|u|}$, which determine the r.m.s. tree sway σ_θ, are in excellent agreement with measurements.

But our cutblock flow observations at Manning are from a single height, so that despite the simplicity of the WFR wind model, there is an enormous disparity between the prolific model output (complete spatial fields of U, V, W, P, k, ε, λ and much more) and the available data to judge its accuracy. To some extent we addressed that deficiency by comparing simulations against the more-complete observations of Raupach et al. (1987). Nonetheless many readers, and especially those very conversant with numerical flow models, may wonder whether the ability of the model to calculate the spatial fields of the mean wind, TKE and wind-force variance represents actual skill, or just judicious selection of model output. That disquieting possibility resonates in our own minds too, for certainly the model results shown are but the 'tip of a paperberg' calculated; and we did specify $c_d ah$ and γ to optimise model agreement with our cutblock data. It may be useful, then, to address the issue of our own objectivity. *How critically* have we compared model results with data? What reassurances can we give that this model is not a slippery thing, that would conform to any data? These points are pertinent:

- We chose maximal *simplicity* in the flow modelling[3], to minimise the introduction of flexible parameters.
- We insisted on constancy of the two unknown (thus free to be optimised) parameters ($c_d ah$, γ) across both our experimental configurations.
- We acknowledged the role of those constants in adjusting 'model curves' toward the data.
- We displayed the modelled and observed fields so as to clearly display *differences*.
- We used a *single normalising scale*, external to the test cutblocks, so as to avoid imparting any misleading appearance of quality to the simulations[4].
- We included *new, testable predictions* of the model.

In short, although the success of the simulations is assuredly not automatic, and depends on the experience of the user to apply the model appropriately, making necessary judgements especially where important input data are uncertain, it remains that *given* a set of inputs, the model is completely objective and reproducible.

In all probability one could invoke a more complex treatment of the Manning flow, and attain better agreement with observations. For example, there is simply no basis to insist that $c_d a$ is constant with position (except in cutblocks, where it vanishes); this was a noticeably inhomogeneous forest. At the very least, leaf area density in the aspen forest is strongly height-dependent (e.g. Amiro, 1990), peaking well below mean tree height: perhaps through having adopted a height-independent (bulk) drag parameter,

[3]An exception is our having carried a full boundary-layer, and Coriolis force. Our first simulations of the Manning flow assumed shear stress to be height-independent (except where disturbed by the forest clearings) to the top of the computational domain, placed at $z/h = 40$; i.e. we ignored large scale pressure gradients, and the Coriolis force, and entirely neglected the crosswind component V. Interestingly, just as WFR found it non-essential to properly model the outer region of their wind-tunnel boundary layer, we found that nothing vital was gained by adding proper PBL structure – other than the assurance we had done the right thing, and the revelation that mean wind direction may swing drastically within the canopy layer.

[4]Whereas in Wilson and Flesch (1996) we unnecessarily introduced independent normalisations for mean wind and for TKE, such that *both* modelled quantities were forced into agreement with observation at one point *within* the cutblock.

we should have also used an *effective* or *aerodynamic* canopy height (h) that is lower than the 'visual' or sampled tree height. It seemed to us better to neglect such options, and show these less-than-perfect outcomes, which nevertheless seem quite realistic, and useful as regards the pattern of tree sway. We look forward to experimental confirmation or contradiction of the untested prediction of Section 7 that in the context of windthrow of remant spruce, wider shelter-strips may function less-effectively than narrow.

In conclusion, given the apparent ability of our wind flow model to diagnose velocity statistics within cutblocks, and the relationship we have established between tree sway and the wind, we feel hopeful that a wind model *can* be a useful tool for identifying effective cutblock designs. No doubt mesoscale meteorological events, possibly in interaction with topographic complexities ignored here, lend a sporadic, unpredictable complexity to the pattern of windthrow. And of course, spatially-varying soil and tree properties must distort our simple picture. Nevertheless we expect that underlying such randomness, and visible in the long term, there will exist a spatial pattern in tree windthrow that is governed by 'routine' wind dynamics, as captured in such models as we described. That blow-down pattern should correlate with long-term spatial trends in the central-tendency statistics we considered, the r.m.s. tree sway (σ_θ), and its surrogate the r.m.s. wind force ($\sigma_{u|u|}$).

Acknowledgements

Funding was provided by the Manning (Alberta) Diversified Forest Trust Fund, and Forestry Canada; and JDW acknowledges research grants from NSERC (Natural Sciences and Engineering Research Council of Canada) and Environment Canada. We are grateful to Dr. S. Navratil and L. Brace for helping us initiate the project, and to T. Thompson for his help in the field.

Appendix A

Relative impact of wind statistics on r.m.s. wind force

Eq. (1) for the specification of the root-mean-square wind force $\sigma_{u|u|}$ involves the mean wind velocity U, the variance σ_u^2, the skewness Sk_u and the kurtosis Kt_u. Is it equally important to specify each of these accurately?

The differential $\mathrm{d}\sigma_{u|u|}^2$ may be expressed as

$$\frac{\mathrm{d}\sigma_{u|u|}^2}{\sigma_{u|u|}^2} = \frac{a_U(\mathrm{d}U/U)+a_\sigma(\mathrm{d}\sigma_u/\sigma_u)+a_S\mathrm{dSk}_u+a_K\mathrm{dKt}_u}{(\mathrm{Kt}_u-1)+4(U/\sigma_u)^2+4(U/\sigma_u)S}$$

where the coefficients of the numerator are

$$a_U = 8\left(\frac{U}{\sigma_u}\right)^2+4\left(\frac{U}{\sigma_u}\right)\mathrm{Sk}_u,$$

$$a_\sigma = 4(\mathrm{Kt}_u-1)+8\left(\frac{U}{\sigma_u}\right)^2+12\left(\frac{U}{\sigma_u}\right)\mathrm{Sk}_u,$$

$$a_S = 4\left(\frac{U}{\sigma_u}\right),$$

$$a_K = 1$$

With $\mathrm{Kt}_u = 4$, $\mathrm{Sk}_u = 1$, and $U/\sigma_u = 1$, values that are typical of our clearing flows, we evaluated the partial fractional changes $d\sigma_{u|u|}^2/\sigma_{u|u|}^2$ caused by 10% changes in each of U, σ_u, Sk_u and Kt_u, i.e. by $\mathrm{d}U/U = 0.1$, etc. The outcomes, in order of increasing fractional response, were as follows: 1% response to 10% in Kt_u, 4% response to 10% in Sk_u, 11% response to 10% in U, and 28% response to 10% in σ_u.

Appendix B

Role of the Coriolis force in canopy flows

The canopy 'wind spiral' has received little attention despite Shinn's (1971) early recognition of it, an exception being Holland (1989). Its origin is simple to give in qualitative terms: deep enough within a dense canopy ($z < h$) the Coriolis force and the turbulent shear-stress are 'small,' and it follows that the mean wind is directed *parallel* to the large scale pressure gradient, implying (up to) a full 90° swing in direction between the Geostrophic-level, where the wind blows perpendicular to the pressure gradient, and ground-level. Shinn used the term 'Quasi-Geotriptic' to describe that local force-balance, "a balance of the drag force and the pressure gradient force but with residual effect of the Coriolis force evident in the direction of the wind drift with respect to the geostrophic definition of the pressure gradient direction."

Dramatic directional shear is presumably then to be regarded as *normal*, in mid- and high-latitude canopies. It will have to be accounted for in scientific descriptions of many problems, e.g. short range patterns of (pollen, seed, etc.) dispersion from localised sources. As regards forest-edge flows, we infer the force-balance may involve both horizontal velocity components in an essential way, i.e. changes coupled through the Coriolis force may be important even when the flow has along-edge symmetry ($\partial/\partial y = 0$).

Appendix C

Diagnosing velocity skewness

Our basis for determination of the alongwind velocity skewness $Sk_u = \langle u'^3 \rangle / \sigma_u^3$ was a simplified transport equation suggested by Hanjalic and Launder (1972), Appendix A (hereafter HL). Our disturbed canopy flow is more complex than the wall boundary-layer flow considered by HL, but we nevertheless adopted their analysis without change. As our closure resolved total TKE (k), but not the separate components σ_u^2 (etc.), we assumed that *equilibrium* partitioning of TKE prevailed throughout our disturbed flow, i.e. that everywhere

$$\sigma_u^2 \equiv \langle u'^2 \rangle = \alpha_u k \tag{A1}$$

Here $\alpha_u = c_e c_u^2$, $c_u \approx 2$ being the equilibrium value of the ratio σ_u/u_{*0}. The HL analysis, so simplified, results in the following transport equation for our two-dimensional, steady state case

$$U\frac{\partial \langle u'^3 \rangle}{\partial x} + W\frac{\partial \langle u'^3 \rangle}{\partial z} = -3\alpha_u^2 k \frac{\partial k}{\partial x} - 3\alpha_u \langle u'w' \rangle \frac{\partial k}{\partial z} - \frac{1}{c_s'}\frac{\varepsilon}{k} \tag{A2}$$

and implies that in undisturbed flow (i.e. setting $\partial/\partial x = 0$),

$$\mathrm{Sk}_u = -\kappa \frac{\langle u'w' \rangle}{\varepsilon\sqrt{k}} \frac{\partial k}{\partial z} \tag{A3}$$

where $\kappa = 3c_s'\alpha_u^{-1/2}$. According to Eq. (A3), the sign of Sk_u is controlled by the vertical gradient in TKE. This is surely an oversimplification, but we found that with $\kappa = 1$ (i.e. $c_s' = \alpha_u^{1/2}/3$), Eq. (A3) gives a good prediction of the equilibrium velocity skewness in and above a model canopy in a wind tunnel.

For disturbed flows, after first obtaining the velocity and TKE fields, we solved Eq. (A2) for skewness. We added small artificial diffusion terms to Eq. (A2) and followed the numerical practise that is standard under SIMPLE.

References

Amiro, B.D., 1990. Comparison of turbulence statistics within three boreal forest canopies. Boundary Layer Meteorol. 51, 99–121.

Blakadar, A.K., 1962. The vertical distribution of wind and turbulent exchange in a neutral atmosphere. J. Geophys. Res. 67, 3095–3102.

Chen, J.M., Black, T.A., Novak, M.D., Adams, R.S., 1995. A wind tunnel study of turbulent airflow in forest clearcuts. In: Coutts, M.P., Grace, J. (Eds.), Wind and Trees, Chap. 4. Cambridge University Press, London.

Delage, Y., 1974. A numerical study of the nocturnal atmospheric boundary layer. Q. J. R. Met. Soc. 100, 351–364.

Finnigan, J.J., Brunet, Y., 1995. Turbulent airflow in forests on flat and hilly terrain. In: Coutts, M.P., Grace, J. (Eds.), Wind and Trees. Cambridge University Press, UK, pp. 3–40.

Flesch, T.K., Wilson, J.D., 1999a. Wind and Remnant tree sway in forest cutblocks. I. Measured winds in experimental cutblocks. Agric. For. Meteorol. 93, 229–242.

Flesch, T.K., Wilson, J.D., 1999b. Wind and remnant tree sway in forest cutblocks. II. Relating measured tree sway to wind statistics. Agric. For. Meteorol. 93, 243–258.

Green, S., Hutchings, N., Grace, J., 1994. Modelling turbulent airflow in sparse tree canopies. Preprint volume (pp. 86–87), 21st Conference on Agric. Forest Meteorol., Am. Met. Soc. San Diego.

Hanjalic, K., Launder, B.E., 1972. A Reynolds stress model of turbulence and its application to thin shear flows. J. Fluid Mech. 52, 609–638.

Hinze, J.O., 1975. Turbulence. McGraw-Hill. ISBN 0-07-029037-7.

Holland, J.Z., 1989. On pressure-driven wind in deep forests. J. Appl. Meteorol. 28, 1349–1355.

Li, Z.J., Miller, D.R., Lin, J.D., 1985. A first-order closure scheme to describe counter-gradient momentum transport in plant canopies. Boundary Layer Meteorol. 33, 77–83.

Li, Z., Lin, J.D., Miller, D.R., 1990. Air flow over and through a forest edge: a steady state numerical simulation. Boundary Layer Meteorol. 51, 179–197.

Liu, J., Chen, J.M., Black, T.A., Novak, M.D., 1996. E–ε modelling of turbulent airflow downwind of a model forest edge. Boundary Layer Meteorol. 77, 21–44.

Miller, D.R., Lin, J.D., Lu, Z.N., 1991. Airflow across an alpine forest clearing: a model and field measurements. Agric. Forest Meteorol. 56, 209–225.

Navratil, S., Brace, L.G., Sauder, E.A., Lux, S., 1994. Silivicultural and harvesting options to favor immature white spruce and aspen regeneration in boreal mixedwoods. Information Report NOR-X-337, Northern Forestry Centre, Canadian Forest Service.

Patankar, S.V., 1980. Numerical Heat Transfer and Fluid Flow, Hemisphere Publ. Co. ISBN 0-07-048740-5.

Raupach, M.R., Bradley, E.F., Ghadiri, H., 1987. Wind tunnel investigation into the aerodynamic effect of forest clearing on the nesting of Abbott's Booby on Christmas Island. Internal report, CSIRO Centre for Environmental Mechanics, Canberra.

Raynor, G.S., 1971. Wind and temperature structure in a coniferous forest and a contiguous field. Forest Sci. 17, 351–363.

Schilling, V.K., 1991. A parameterization for modelling the meteorological effects of tall forests – a case study for a large clearing. Boundary Layer Meteorol. 55, 283–304.

Svensson, U., Haggkvist, K., 1990. A two-equation turbulence model for canopy flows. J. Wind Eng. Indust. Aero. 35, 201–211.

Shinn, J.H., 1971. Steady-state two-dimensional air flow in forests and the disturbance of surface layer flow by a forest wall. Ph.D. Thesis, University of Wisconsin, Madison, 91pp.

Takahashi, H., 1978. Wind tunnel test on the effect of width of windbreaks on the wind speed distribution in leeward. J. Agr. Met. (Japan) 33, 183–187.

Wang, H., Takle, E.S., 1996. On three-dimensionality of shelterbelt structure and its influences on shelter effects. Boundary Layer Meteorol. 79, 83–105.

Wilson, J.D., Flesch, T.K., 1996. Diagnosing wind variation in periodic forest clearcuts, in relation to tree sway, preprint volume, 22nd Conference on Agricultural and Forest Meteorology, Am. Meteorol. Soc. pp. 387–390.

Wilson, J.D., Finnigan, J.J., Raupach, M.R., 1998. A first-order closure for disturbed plant-canopy flows, and its application to winds in a canopy on a ridge. Quart. J.R. Meteorol. Soc. 124, 705–732. See also Preprint Volume, 11th Symposium of the AMS on Boundary Layers and Turbulence, pp. 539–542.